International Journal of Multiphase Flow 133 (2020) 103460

Contents lists available at ScienceDirect

International Journal of Multiphase Flow

journal homepage: www.elsevier.com/locate/ijmulflow

An improved multi-scale two phase method for bubbly flows

Xiaosong Zhang[a,b], Jianhua Wang[a], Decheng Wan[a,*]

[a] Computational Marine Hydrodynamics Lab (CMHL), School of Naval Architecture, Ocean and Civil Engineering, State Key Laboratory of Ocean Engineering, Shanghai Jiao Tong University, Shanghai 200240, China
[b] CSIC Shanghai Marine Energy Saving Technology Development Co.,Ltd, No.185 Gao Xiong Road, Shanghai, China

ARTICLE INFO

Article history:
Received 16 June 2020
Revised 2 September 2020
Accepted 7 September 2020
Available online 10 September 2020

Keywords:
Multi-scale two phase flow
VOF-Euler-Lagrange coupling
Transformation criteria
Curvature-based algorithm

ABSTRACT

Multiple spatial scale is an important characteristic of two phase flow phenomena. The micro-scale and macro-scale flow structures are obviously different in flow state and have different effects on the mass, momentum and energy transfer between two phases. Different modeling approaches have been developed for each scale physical phenomenon in traditional numerical simulations. However, it is difficult to simulate two phase flow systems with multi-scale flow structures simultaneously. In order to address this problem, a multi-scale two phase method is developed based on the combination of Volume of Fluid (VOF) interface capture method and Euler–Lagrange particle tracking method. The fundamental assumption of the present method is that there is a clear scale separation between VOF interfaces and bubbles. Therefore, VOF method with artificial compressive algorithm is used to simulate the dynamic evolution of macro-scale air-water interface. While Euler–Lagrange method is used to track the micro-scale bubbles that cannot be captured in grids. Collision, coalescence and breakup of Lagrange bubbles and two-way coupling are fully considered to construct a comprehensive micro-bubble solving procedure. Transformation criteria and the corresponding algorithms between micro-scale and macro-scale flow structures are designed and discussed in detail. In addition, a new curvature-based algorithm for the transformation from VOF interface to Lagrange bubbles is proposed. Simulations of typical two phase flow problems involving multi-scale flow transformation are carried out to test the performance of the multi-scale solver. Results indicate that the multi-scale two phase method performs significantly better than the pure VOF method in capturing micro-scale phenomena. Besides, the curvature-based transformation algorithm proposed in this paper is proved to be more precise and efficient than the previous identify-based one. From the perspective of simulation accuracy and efficiency, the multi-scale two phase method is more promising for the simulation of actual complex two-phase flows.

1. Introduction

Many two-phase flow problems present obvious multi-scale characteristics due to the existence of bubbles, droplets and large interface. Typical multi-scale two phase flow problems include jet atomization (Dumouchel et al., 2015), bubble plume (Liu et al., 2004; Yang et al., 2011), cavitation (Kuiper, 2010) and wave breaking (Deike et al., 2016). Fig. 1 illustrates the flow characteristics of multi-scale two-phase flow by taking a simple bubble plume problem as an example. Gas is injected into the liquid field from the bottom inlet, micro-scale bubbles, macro-scale bubbles and gas-liquid free surface are present in the flow field at the same time. Continuous interface deformation occurs in the process of macro-scale bubbles moving, at the same time smaller bubbles break off from large bubbles under the influence of flow interaction. Micro-scale bubbles keep constant shape and present a chaotic motion. Two phase flow at different scales presents different characteristics, which have an important effect on the mass, momentum and energy transfer.

Numerical simulation has been widely used in predicting and investigating two phase flow problems nowadays. Different modeling methods are developed for two-phase flow problems at different scales. On the one hand, several mature interface capture methods have been applied to the macro-scale two phase flow problems successfully. For example, ocean waves simulated by Volume of Fluid (VOF) method (Lubin, et al., 2015) and Level-set method (Bihs et al., 2016), complex droplet motion simulated by Front-Tracking Method (FTM) (Armandoost et al., 2018), and impact dynamics of compound drop simulated by Diffuse -Interface Method (Liu et al., 2018). On the other hand, Two-Fluid Method (TFM) and Euler–Lagrange method are two classical numerical

* Corresponding author.
E-mail address: dcwan@sjtu.edu.cn (D. Wan).

https://doi.org/10.1016/j.ijmultiphaseflow.2020.103460
0301-9322/

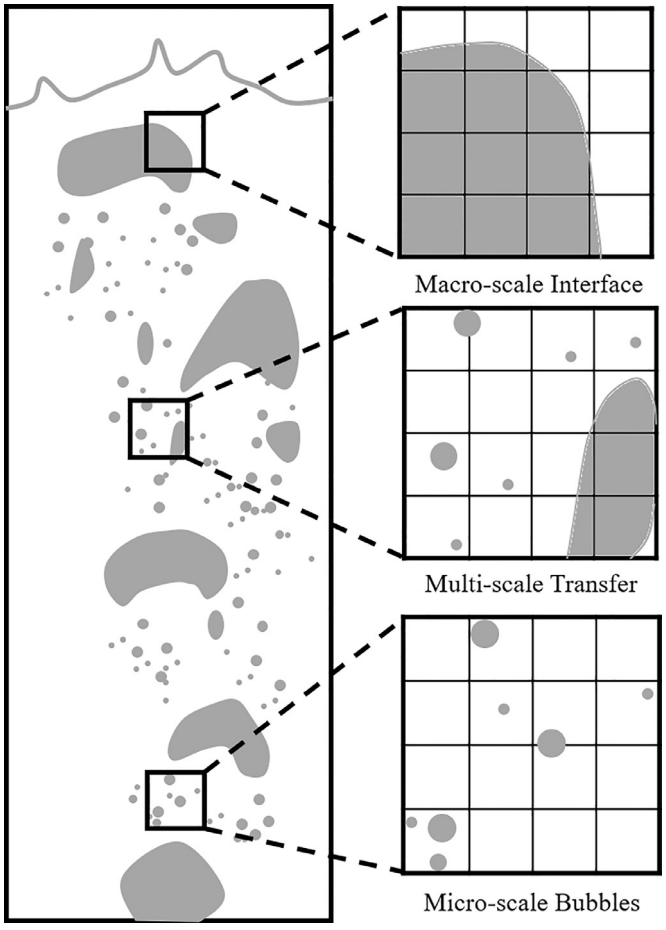

Fig. 1. Representation of the multi-scale aspect of bubble plume.

methods for two phase flow problems with a continuous phase and a discrete phase consisting of large amount of micro-scale particles. The TFM has been widely used in the prediction of dense bubbly flow (Ma et al., 2015a). And the Euler–Lagrange method provides a more precise solution for bubble dynamics by individually tracking (Ma et al., 2015b). These numerical methods perform well in reproducing typical physical problems and have been widely validated. However, two phase flow problems with multiple scales have become a challenge to the numerical simulation. The grid-based interface capture method is difficult to capture a large number of micro-scale structures due to the limitation of computational cost. While the approximation methods cannot simulate the dynamic evolution of larger air-water interface. In recent years, several hybrid numerical simulation methods have been proposed to solve the multi-scale flow. By assuming that there is a clear scale separation between large interfaces and small bubbles, droplets and particles, the single-scale numerical methods mentioned above were combined to solve flow field at different scales in a system. At the same time, transformation algorithms were designed to achieve smooth multi-scale coupling.

The idea of concurrent coupling of different simulation methods for studying the multiple spatiotemporal behavior has been adopted in various physical problems. In terms of microfluid and nanofluid, multi-scale ideas were used to develop hybrid atomistic-continuum methods for dense fluids (Mohamed and Mohamad, 2010). Domain-decomposition-based algorithms were used to solve th multiscale flow. Besides, many general single-phase problems also contain phenomena in different spatial scales, such as the thermal management in the data center (Alkharabsheh et al., 2015) and the mass transfer in fuel cells (Grew and Chiu, 2012). Tong et al. (2019) summarized the combined application of different scale methods on these problems in detail. In addition, the multi-scale simulation idea has also been used in granular flow problems (Chen et al., 2016, 2017, 2018). By the combination of discrete method and continuum method in different region, the computational efficiency was significantly improved. In conclusion, the idea of multi-scale numerical simulation has been applied to several kinds of fluid dynamic problems due to its advantages in computational accuracy and efficiency. In this paper, the authors mainly focus on the multi-scale bubbly flows, in which the evolution of air-water interface is the macro-scale phenomenon and discrete bubbles are the micro-scale phenomenon. Next, the development of multiscale numerical simulation methods for air-water two phase system will be reviewed.

There are great differences in the modeling ideas and simulation effects between Euler Two Fluid Method and Euler–Lagrange method, directly leading to the differences in the development of multi-scale two phase flow solvers based on them. The motion of dense discrete phase is assumed to be continuous in the TFM, therefore the Navier–Stokes equations are also used as the governing equations of discrete phase. Ma et al. (2011a) combined the TFM and interface capture method based on Level-set and carried out a multi-scale simulation of the hydraulic jump phenomenon. Wave-induced bubble sources in the recirculation region and turbulent shear region were captured by the TFM, while free surface was captured by Level-set method. A comprehensive subgrid air entrainment model designed for the multi-scale simulation was adopted to predict the bubble entrainment rate (Ma et al., 2011b). Although the solution framework is one-way coupled, the simulation effect has made a unique breakthrough. VOF method is another commonly used interface capture method. Yan and Che (2010) developed a multi-scale two phase flow solver based on the combination of VOF and TFM. Flow field in the algorithm was divided into three phases according to the length scale. Special treatment of "volume fraction redistribution" was implemented. Bubbly flow followed by a rising large gas bubble in a vertical pipe was simulated in their study. Wardle and Weller (2013) improved the TFM-VOF method by increasing the accuracy of interface capturing. Liquid-liquid extraction simulations were performed to verify the capacity of the method in predicting discrete phase distribution. Multiple Size Group (MUSIG)-model was added into a multi-scale solver by Hänsch et al. (2012) to describe the mass transfers between different bubble size groups due to coalescence and breakup as well as gas-liquid transfers. Closure models between the multi-scale flows were designed using basic ideas of the AIAD-model (Höhne et al., 2011). Volume fraction fields in a bubble column domain is simulated to verify the solver. Similar AIAD-model was used by Schmidtke and Lucas (2008) to simulate bubble entrainment by an impinging jet. The TFM method was used to reproduce the physical process of bubble generation near the jet, which cannot be captured by macro-scale simulation. A coupled MUSIG-VOF approach is developed by Xiang et al. (2014) to handle the formation of large-scale free surface, bubble entrainment and bubble dispersion in hydraulic oscillating jumps. The predicted void fraction bubble frequency distributions were in good agreement with experimental measurement. Rezende et al. (2015) developed a two-fluid model with a tensor closure model approach to improve the accuracy of the traditional single-scale interface capture method. The air-water mixing phenomenon caused by interface breakup is simulated much better.

Using the TFM method to describe the bubble and droplet groups in multi-scale flows can give the general phase fraction and momentum distribution, but the motion details of discrete phase cannot be obtained. In contrast, micro-scale flow structures are tracked individually in Euler–Lagrange method, which can be

used to analyze the behavior and physical mechanism of micro-scale bubbles and droplets. Herrmann (2010) developed a parallel Level-set/Euler–Lagrange multi-scale coupling procedure. The simulated flow scale is related to the grid scale. The level-set method is used to capture the flow structures with sufficient number of occupied grids for fully resolving. In the flow regions where the phase interface geometry can no longer be resolved adequately, the micro-scale flow structures were modeled as Lagrange particles. By using this method, the simulation accuracy of jet atomization process was improved obviously. Patkar et al. (2013) presented a hybrid Lagrange–Euler framework for multi-scale bubbly flow simulation. The larger well-resolved bubbles were modeled by Level-set method and the smaller under-resolved bubbles were modeled by Lagrange tracking. Novel interconverting scheme and seeding mechanism models were proposed to simulate complex interaction. Elaborate direct numerical simulations were performed for rising bubble breakup, bubble plume, cavitation and faucet pouring water problems. Hsiao et al. (2013) carried out both experimental measurement and Euler–Lagrange one-way coupled multi-scale simulation for horizontal plunging jet flow. Bubble entrainment was simulated by an improved sub-grid bubble entrainment model. The evolution of free-surface and micro-bubbles were in good agreement with the experimental results. Cavitation flow involves multi-scale flow states, including micro-scale gas core, sheet cavity, dispersing bubble cloud. Coupled Euler–Lagrange/Level-set method provides a solving approach for the whole process simulation of cavitation flows (Ma et al., 2017; Hsiao et al., 2017). By using the multi-scale method, the capture accuracy of the flow structures is obviously improved, such as cavitation collapse on hydrofoil surface and tip vortex cavitation of propeller. At the same time, the pressure oscillation is also well predicted.

The combination of VOF method and Euler–Lagrange method is also an effective idea of constructing multi-scale algorithm. Compared with the Level-set method, the VOF method has significantly better conservation. Jain et al. (2014) developed a semi-coupled VOF/Euler–Lagrange multi-scale two phase flow solving code for bubble plume problems. The free surface was captured by VOF method while bubbles in water were modeled by Lagrange tracking. Transformation from Lagrange bubbles to VOF interface was implemented when bubbles approach to free surface. However, micro-bubbles generated by interface breakup or deformation of large bubble due to coalescence were not considered. Similar numerical method was adopted by Li et al. (2017) to study gas-steel-slag three-phase flow in ladle metallurgy. The perturbations caused by the rise of Lagrange bubbles to the free surface were analyzed in detail. To further simulate complex physical phenomena, several scholars developed fully-coupled VOF/Euler–Lagrange multi-scale two phase flow solving code. Tomar et al. (2010) performed multi-scale simulations of primary atomization using a VOF algorithm coupled with a two-way coupling Lagrange particle tracking model. Conversion between VOF interface and Lagrange particles was achieved by the manipulation of local void fraction and particle volume. Transformation from VOF framework to Lagrange framework was identified by tagging simply connected cells with void fraction larger than zero. At the same time the transform criterion from Lagrange framework to VOF framework was based on the proximity with interface. The algorithm has been successfully used in the prediction of jet atomization. More recently, Ling et al. (2015) improved the VOF-EL multiscale algorithm by determining the criteria for conversion. In their study, VOF bubbles or droplets which contain less than 4^3 grids and are more than one diameter away from interface should be transformed to spherical Lagrange points. In turn, Lagrange particles with a distance less than one diameter from the interface will be transformed back to VOF solution. Karimi et al. (2018) carried out polyurethane foam simulation using VOF-EL multi-scale method. The numerical results were in good agreement with experimental results. Zuzio et al. (2018) improved the accuracy of multi-scale algorithm. An adaptive mesh refinement technique is used to dynamically optimize the structured Cartesian mesh and improve the interface capture accuracy. It was proved that the combination of Lagrange tracking could improve the computational efficiency on the basis of micro-scale structure simulation.

Summing up the above numerical simulation methods, the Euler–Lagrange method can track each micro-scale flow structure in detail, and the VOF method has good conservation. Therefore, these two methods are used as the basic methods for constructing the multi-scale two-phase flow solver in this study. The previous VOF/Euler–Lagrange multi-scale studies are not comprehensive enough about the consideration of physical phenomena. For example, the semi-coupling (Jain et al., 2014; Li et al., 2017) and partially ignoring kinematic behaviors of bubbles and droplets (Tomar et al., 2010; Ling et al., 2015; Zuzio et al., 2018). The fundamental goal of the present work is to develop a comprehensive multi-scale two phase solver based on VOF and Euler–Lagrange method for bubbly flow problems. Collision, coalescence and breakup of Lagrange bubbles are considered and high robustness two-way coupling algorithm is adopted in the Euler–Lagrange solving framework. Specific multi-scale transformation algorithms are designed to guarantee the smooth transformation between VOF interface and Lagrange bubbles. On the basis, this paper focuses on the discussion of simulation effects, efficiency, critical criteria and algorithm performance of the developed multi-scale solver.

The paper is organized as follows. First, the single-scale numerical methods used to construct multi-scale method in this work are introduced in Section 2 and Section 3, including the VOF interface capture algorithm and Euler–Lagrange algorithm for small bubble tracking. Algorithms of Lagrange bubble collision, coalescence and breakup are also introduced. Section 4 describes the multi-scale transformation algorithm and the overall computational procedure. Next, some academic two phase problems are simulated to show the capability of the present method in the description of multi-scale phenomena. The effects of critical criteria and transformation algorithms are discussed in detail. Finally, conclusions are provided.

2. Mathematical modeling for Euler framework

In the present solver, large air-water interfaces and small bubbles are modeled separately according to different scales. Macro-scale flow is solved in the Euler framework based on grids. Detailed mathematical models for Euler framework including governing equations and interface capture method are introduced as follows.

2.1. Governing equations

The two phase flow considered in the present study is assumed to be incompressible and immiscible. The adopted governing equations are Navier-Stokes equations consist of continuity equation and momentum equation as follows:

$$\frac{\partial \alpha_L}{\partial t} + \nabla \cdot (\alpha_L U) = 0 \tag{1}$$

$$\frac{\partial \alpha_L \rho U}{\partial t} + \nabla \cdot (\rho U U) = -\nabla p + \rho g + \nabla \cdot S + f_S + f_B \tag{2}$$

where $\boldsymbol{U}$ is fluid velocity vector, ρ is the fluid density, p is pressure, $\boldsymbol{g}$ is gravity, $S = 2\mu D$ with $D = 1/2(\nabla U + \nabla U^T)$ is the viscous stress. f_B is the Euler–Lagrange coupled source term, which reflects the effect of micro-bubbles on the fluid. f_S is surface

tension force, which is defined as:

$$f_S = \sigma k \nabla \alpha_V \tag{3}$$

where σ is surface tension coefficient, which is set to be 0.072 N/m in the present study. k is interface curvature.

It is worth noting that the influence of bubbles at different scales on flow momentum is different. Therefore, the calculation of volume fraction in the grids is also different. There are two kinds of volume fraction in the solving procedure. α_{L} in Eq. (1) and Eq. (2) represents the volume fraction of a grid removing the volume of Lagrange bubbles. While α_{V} in Eq. (3) represents the volume fraction of a grid calculated by the VOF transport equation.

2.2. Interface capture method

The complex evolution of interface is an important feature of macro-scale two phase flow problems. In order to capture the interface accurately, the Volume of Fluid (VOF) method with artificial compressive term is applied to locate and track the air-water interface (Hirt and Nichols, 1981). The transport equation of the volume fraction of water can be written as:

$$\frac{\partial \alpha_V}{\partial t} + \nabla \cdot (\alpha_V U) + \nabla \cdot (\alpha_V (1 - \alpha_V) U_c) = 0 \tag{4}$$

where the third term on the left side of Eq. (4) is the artificial compression term and it is non-zero only at the interface. The effect of artificial compressive term is to counteract the phase interface fuzziness caused by the numerical dissipation to obtain a sharper interface. U_c is the compressive speed, which should be used to compress in the normal direction of the interface rather than tangential, otherwise false diffusion will appear. Therefore the compressive speed is defined as:

$$U_c = c|U| \frac{\nabla \alpha}{|\nabla \alpha|} \tag{5}$$

where c represents compressive factor. The compression effect increases with the increase of c. There is no compressive effect when c equals to 0.

3. Mathematical modeling for Lagrange framework

In the present solver, micro-scale bubbles are tracked individually in Lagrange framework based on Newton's second law. Comprehensive bubble behaviors including collision, coalescence and breakup are modeled in the solving procedure. Detailed mathematical are introduced as follows.

3.1. Micro-bubble advection tracking

Every Lagrange micro-bubble is assumed to be spherical with constant diameter. The advection of bubbles is rigid translation controlled by various hydrodynamic forces and collision force. The governing equation can be written as follows:

$$\begin{aligned} m\frac{dv}{dt} &= f_D + f_L + f_P + f_G + f_C \\ &= \frac{3mC_D}{4d}|u - v|(u - v) + \frac{m\rho_l}{\rho_b} C_L (u - v) \times (\nabla \times u) \\ &\quad + \frac{m\rho_l}{\rho_b}\frac{Du}{Dt} + mg\left(1 - \frac{\rho_l}{\rho_b}\right) + f_C \end{aligned} \tag{6}$$

where $\boldsymbol{v}$ is the velocity of micro-bubble, m is mass, d is bubble diameter, ρ_{l} and ρ_{b} represent the liquid density and bubble density, respectively. Source terms of Eq. (6) represent drag force, shear lift force, fluid acceleration force, gravity-buoyancy and collision force in order.

Two-way coupling between Lagrange bubbles and Euler phase solving is realized by a Gaussian distribution scheme (Zhang et al., 2020). The improved algorithm has been proved to be effective in improving the robustness of the code.

Tomiyama's drag model (Tomiyama et al., 2002a) and lift model (Tomiyama et al., 2002b) are adopted for the calculation of Drag force coefficient $\mathrm{C_D}$ and lift force coefficient C_L as follows:

$$C_D = \max\left(\min\left(\frac{16}{Re}\left(1 + 0.15Re^{0.687}\right), \frac{48}{Re}\right), \frac{8}{3}\frac{Eo}{Eo + 4}\right) \tag{7}$$

$$C_L = \begin{cases} \min\left[0.288 \tan h(0.121Re), f(Eo_d)\right] & Eo_d < 4 \\ f(Eo_d) & 4 \le Eo_d \le 10.7 \end{cases} \tag{8}$$

$$f(Eo_d) = 0.00105Eo_d^3 - 0.0159Eo_d^2 - 0.0204Eo_d + 0.474$$

where $\mathrm{Re} = \mathrm{d}\,|\mathrm{u} - \mathrm{v}|/\nu$ is the bubble Reynolds number, Eotvos number Eo is defined as $\mathrm{Eo} = \mathrm{g}\,|\rho_{\mathrm{l}} - \rho_{\mathrm{b}}|/\sigma$.

3.2. Micro-bubble collision

The collision between two Lagrange micro-bubbles is handled to be an elastic process. Although the bubble deformation is not actually solved, a nonlinear model (Heitkam et al., 2017) is used to describe the relationship between the collision force and the deformation of bubbles. The collision force consists of an elastic force and a viscous force which are defined as:

$$F_{elastic} = 18.5\sigma\left(\frac{\Delta}{R_{eq}}\right)^2 + 2.0\Delta\sigma \tag{9}$$

$$F_{viscous} = uC_{bc}\frac{12\mu_l}{2\pi}0.34\left(\frac{\Delta}{R_{eq}} + 0.0002\right)^{-0.5} \times \left(4.0\sqrt{\frac{R_{eq}^3}{h_0}} + 3.0R_a\frac{R_{eq}}{h_0}\right) \tag{10}$$

where R_{eq} is the effective radius, Δ is the deformation length of bubble, h_0 is the gap width when bubble approaches another bubble or a wall surface. The parameter C_{bc} is a constant collision coefficient, which is equal to 1 for bubble-wall collision and 0.25 for bubble-bubble collision.

3.3. Micro-bubble breakup

Previous Euler–Lagrange multi-scale numerical methods usually ignored the breakup of Lagrange bubbles. In fact, under the effect of turbulent fluctuation and viscous shear stress, Lagrange bubbles can further breakup and form a special size distribution in the flow field. The complex physical breakup mechanism can be described by the relationship with turbulent kinetic energy and bubble surface energy, which can be further derived to be a critical weber number. The critical criterion proposed by Lau et al. (2014) for Euler–Lagrange simulation is adopted in the present solver, which can be written as:

$$We = \frac{\rho_l \overline{\delta u^2(d)} d}{\sigma} > We_{crit} = 12 \cdot \zeta; \zeta = \left(\frac{1 + 2E_b^p}{3E_b^{2/3p}}\right)^{-1/p} \tag{11}$$

where $p = 1.6075$, $E_b = f(Eo_d)$ has been shown in Eq. (8). This model is derived by the analysis of bubble deformation in turbulence flow and has been proved to be accurate.

Another key problem of bubble breakup is the daughter bubble size distribution. Binary breakup is assumed in the present solver and the daughter bubble size is described as a U-shape distribution. The U-shape distribution model has been proved to have a strong physical foundation, which stands for the mechanism that equal size binary breakup consumes the most energy (Nambiar et al., 1992). The probability density function is defined as:

$$f_{bv}(\gamma) = \frac{\Gamma(1)}{\Gamma(0.5)\Gamma(0.5)}\gamma^{-\frac{1}{2}}(1 - \gamma)^{-\frac{1}{2}} \tag{12}$$

where Γ is the gamma function and γ is a random value between 0 and 1.

3.4. Micro-bubble coalescence

Film drainage model (Prince and Blanch, 1990) is adopted in the present solver, which is one of the most widely accepted bubble coalescence models in the previous studies. The dominate mechanism of the model is that there is a thin liquid film between two bubbles when they contact to each other. During the bubble contact process, the liquid film is drained and thinned. Coalescence happens when the liquid film is drained to a critical thickness. Therefore, the critical criterion is that the contact time of two bubbles must be longer than the liquid film drainage time. The drainage time is defined as:

$$t_{drainage} = \sqrt{\frac{d_{eq}^3 \rho_l}{128\sigma}} \ln(\frac{\theta_0}{\theta_f}) \tag{13}$$

where θ_0 and θ_f is the initial liquid film thickness and final liquid film thickness, respectively. θ_0 is set to be 10^{-4} and θ_f is set to be 10^{-8} for air-water system in the present study.

Benefiting from the fact that the contact between bubbles can be calculated directly in the present solver as described in Section 3.2, no additional model is required to calculate the contact time.

4. Transformation algorithm and computational procedure

The detailed numerical methods adopted in the present method for single-scale two phase flow have been introduced in Sections 2 and 3. In this section, the transformation algorithms between the two scale models are explained and the numerical implementation for the main computational procedure is introduced.

4.1. Transformation from Lagrange bubbles to VOF interface

There are two scenarios that Lagrange bubbles should be transformed to VOF interface:

(a) the Lagrange bubbles contact with an existing VOF interface.
(b) the bubbles coalesce and grow so large that they are no longer suitable for tracking in the Lagrange framework.

Illustration of the transformation process for these two scenarios can be seen in Fig. 2. For the first scenario (a), a transformation criterion based on the distance between Lagrange bubble and existing VOF interface is usually adopted. Although this algorithm is relatively simple and straightforward, the definition of critical distance Δ_{BI}^{cri} are different in previous studies. There are mainly three kinds of critical values, which are:

$$\Delta_{BI} < \Delta_{BI}^{cri} = \frac{d}{2} \tag{14}$$

$$\Delta_{BI} < \Delta_{BI}^{cri} = \frac{d}{2} + l_g \tag{15}$$

$$\Delta_{BI} < \Delta_{BI}^{cri} = \frac{d}{2} + 2l_g \tag{16}$$

where d is the Lagrange bubble diameter, l_g is the local interface grid thickness.

Eq. (14) is the most commonly used criterion in the previous studies because of its explicit physical meaning. Eq. (15) and Eq. (16) add the influence of interface grid thickness based on Eq. (14). However, a comparison of the effects of these different critical criteria is still lacking, which becomes an important work of the present study.

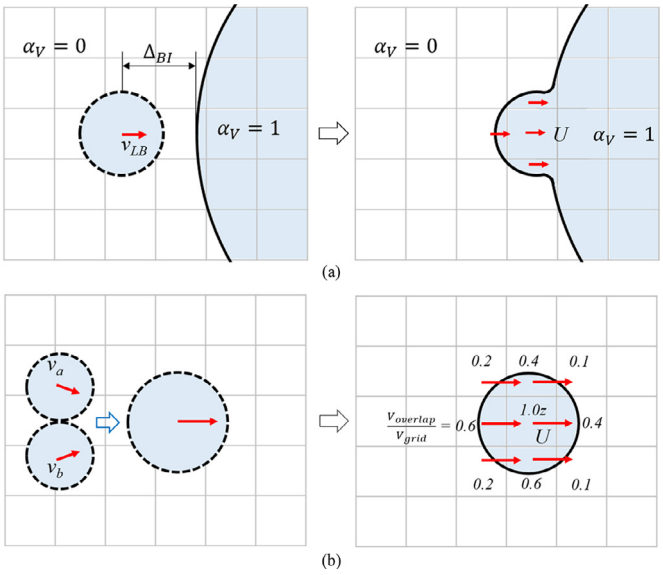

Fig. 2. Illustration of the two kinds of transformation process from Lagrange bubbles to VOF interface. (a) The Lagrange bubbles contact with an existing VOF interface. (b) The bubbles coalesce and grow so large that they are no longer suitable for tracking in the Lagrange framework.

For the second scenario (b), the critical Lagrange bubble size is limited by the bubble diameter and grid size, which can be written as:

$$d > \max(d_{thr}, C_{thr} l_g) \tag{17}$$

where d_{thr} is a threshold bubble diameter and C_{thr} is a user defined threshold grid size factor. The critical diameter of Lagrange bubbles in the transformation algorithm is considered from two aspects. First, in physics, the d_{thr} represents the critical diameter that bubbles can basically maintain a sphere shape in specific physical problem. In other word, d_{thr} is the upper limit of bubble diameter suitable for Lagrange simulation. Therefore, the value of d_{thr} is determined by specific physical problems. In a specific physical condition, bubbles with the diameters larger than d_{thr} deform under the influence of the flow, which does not conform to the spherical hypothesis in the Lagrange framework. Therefore, the Lagrange bubble is transformed to VOF interface. Second, in numerical modeling, because of the relationship between bubble size and grid size, another critical criterion is designed, which is C_{thr} multiplied by l_g. C_{thr} is a threshold grid size factor, which represents the maximum number of grids a Lagrange bubble can contain. When transformation takes place from Lagrange bubble to VOF interface, the bubble should occupy enough grids so that the bubble can be expressed, but not too many grids because of numerical instability in two-way coupling. Therefore, the value of C_{thr} is recommended between 1.0 and 8.0.

The above describes the critical criteria in two different scenarios. With the help of Fig. 2, the implementation of the transformation algorithm is introduced next. The dotted line represents Lagrange bubbles, and the solid line represents VOF interface. Each bubble is traversed at each computation time step to evaluate whether the critical condition of transformation is met. If so, the grids occupied by the bubble will be marked. The volume fraction field will be transformed first. Volume fraction values α_V of the grids contained by the Lagrange bubble are set to be zero. While the α_V value of the grids at the edge of the Lagrange bubble will be determined by the ratio of the overlap volume by the grid volume. The main goal of volume fraction field transformation is to ensure the conservation of mass. At the same time, the computational grids containing the Lagrange bubble are assigned a velocity

field for momentum conservation. For scenario (a), the velocity U in grids are equal to the original velocity of the Lagrange bubble. For scenario (b), the velocity is obtained according to the two small bubbles before coalescence as Eq. (18) shows. After transformation, the original Lagrange bubble will be removed immediately within a time step to achieve a smooth simulation.

$$U = \frac{\left(d_a^3 v_a + d_b^3 v_b\right)}{\left(d_a^3 + d_b^3\right)} \tag{18}$$

4.2. Transformation from VOF interface to Lagrange bubbles

The transformation of micro-scale bubbles from VOF interface to Lagrange tracking can significantly improve the simulation accuracy. At present, most of the transformation algorithms in literatures consist of two steps (Herrmann, 2010; Patkar et al., 2013; Zuzio et al., 2018). First, the VOF bubbles in the computational domain are identified and tagged to calculate the volume and centroid of each bubble. Second, evaluating the size criterion for each VOF bubble to complete the transformation. This method is called identify-based algorithm in this paper. A new curvature-based algorithm is proposed in this paper to provide a lower computational cost and more efficient way for multi-scale bubbly flow simulation. The two algorithms developed in the present solver are introduced as follows.

4.2.1. Identify-based algorithm

The first step of the identify-based algorithm is to detect the VOF bubbles to be transformed. A flood-fill algorithm is adopted in the present solver to identify the volume and centroid of each VOF bubble. Flood-fill is a classical algorithm in image processing and has been widely used in raster graphic editors to color connected areas. Recently, the algorithm was adopted by Wang et al. (2016) and Deike et al. (2016) to identify bubbles in breaking waves. The algorithm is implemented in a stack-based (recursive) fashion and the detailed procedure can be seen in Fig. 3.

First, each cell in the computational domain is looped over and evaluated whether the volume fraction α_V is smaller than 0.5. If the criterion is true, the main loop is paused and the cell is tagged with a unique number n. Then, loop over the neighbor cells of the initial cell and seek the cells located in the same bubble with the initial cell. A recursive idea is taken to advance the search for neighbor grids until all the cells in one bubble have been tagged with the same number as the initial cell, which is shown in Fig. 3(c). After the process above, this one bubble is identified completely. The main loop continues to identify the next bubble $n + 1$. After the identification, three important information, volume, centroid and the contained grid number, are stored for each VOF bubble b. The volume and centroid can be calculated by:

$$V_b = \sum_{i \in N_b} V_{cell}^i \left(1 - \alpha_v^i\right) \tag{19}$$

$$X_b = \frac{1}{V_b} \sum_{i \in N_b} V_{cell}^i \left(1 - \alpha_v^i\right) X_{cell}^i \tag{20}$$

where V_{cell} and X_{cell} is the volume and centroid of the grid-cell, respectively. It should be noted that there is some error in the current bubble identify algorithm, which comes from the grids partially occupied by the VOF interface on the bubble surface.

The transformation criterion can be defined directly based on the geometric information of VOF bubbles. N_b is defined as the total number of cell contained in a bubble. Small bubbles with $N_b < N_{cri}$ can be transformed to Lagrange tracking. The critical number N_{cri} is determined by specific computational requirements. A larger number of N_{cri} results in that larger deformable VOF bubbles are transformed to spherical Lagrange bubbles, reducing the accuracy of simulation and producing numerical instability in the Euler–Lagrange two-way coupling. Zuzio et al. (2018) used $N_{cri} = 8^3$ in their study.

If a VOF bubble satisfies the critical criterion and will be transformed into a Lagrange bubble, the volume fraction field α_V of the grids occupied by the VOF bubble will be set to 1 firstly. Volume and location of the new Lagrange bubble are determined by Eqs. (19) and (20). At the same time, velocity of the new Lagrange bubble is obtained by averaging the velocity field of the VOF bubble as Eq. (21) shows.

$$v_b = \frac{1}{V_b} \sum_{i \in N_b} V_{cell}^i \left(1 - \alpha_v^i\right) U_{cell}^i \tag{21}$$

4.2.2. Curvature-based algorithm

As mentioned above, the identify-based transformation algorithm needs to identify the VOF bubbles in the flow field at each time step, which involves a large number of loops, resulting in a significant increase of computational costs. At the same time, it will also consume a large amount of computer memory if there are large bubbles containing a large number of grids. Therefore, the authors proposed a curvature-based algorithm to provide a high-efficiency method for the transformation from VOF interface to Lagrange bubbles.

If a continuous air-water interface is about to break up into small bubbles, the location where the interface is broken is bound to form a bulge, leading to the difference of curvature at different locations as Fig. 4 shows. The curvature of the interface is larger for the bulge and the small bubbles generated by breaking. Therefore the curvature can be used as a criterion for the transformation from VOF interface to Lagrange bubbles. However, it is difficult to evaluate the range of curvature. Thus, the curvature radius R_c, which is equal to the radius of inscribed sphere, is adopted as the geometrical criterion of transformation. Besides, there is a momentum criterion that the velocity of the bulge must be towards the outside of the VOF interface. In conclusion, the critical criterion in the curvature-based algorithm can be written as:

$$(0 < \alpha_v < 1) \&\& (R_c < R_c^{cri}) \&\& (U_n \cdot \hat{n} > 0) \tag{22}$$

where R_c^{cri} is a critical curvature radius value determined by desired transformation scale in specific simulations. U_n is the velocity of the interface and $\hat{n}$ is the unit normal vector of the interface. For the implementation of the algorithm, it only takes one loop of grid and the computational cost will not increase significantly.

After the transformation is implemented, all the Lagrange bubbles are in sub-grid scale firstly. Volume, location and velocity are determined by the void fraction, center coordinate and velocity of the grids on the broken VOF interface, respectively. It should be noted that this breakup and transformation are reasonable in a violent turbulent flow, but in more moderate flows it may imply excessive breakup because the bubbles are too small. By adopting the Lagrange bubble coalescence algorithm as Section 3.4 shows, small bubbles in the moderate flow will coalesce within several time steps, which improve the simulation effect. In contrast with the Identify-based algorithm, the conservation error caused by the identify can also be avoided, which reduces the air mass loss in the flow field.

Another problem for this algorithm is the calculation of curvature. The calculation of interface normal vector and curvature needs to take the derivative of volume fraction α_V in the VOF method. It is well known that the curvature calculation error in the VOF method is large because α_V is a discontinuous function. A simple coupled Level-set Volume of Fluid (S-CLSVOF) method proposed by Albadawi et al. (2013) is adopted in the present solver to overcome the problem of curvature calculation. A Level-set distance function field ϕ is introduced and the interface is defined

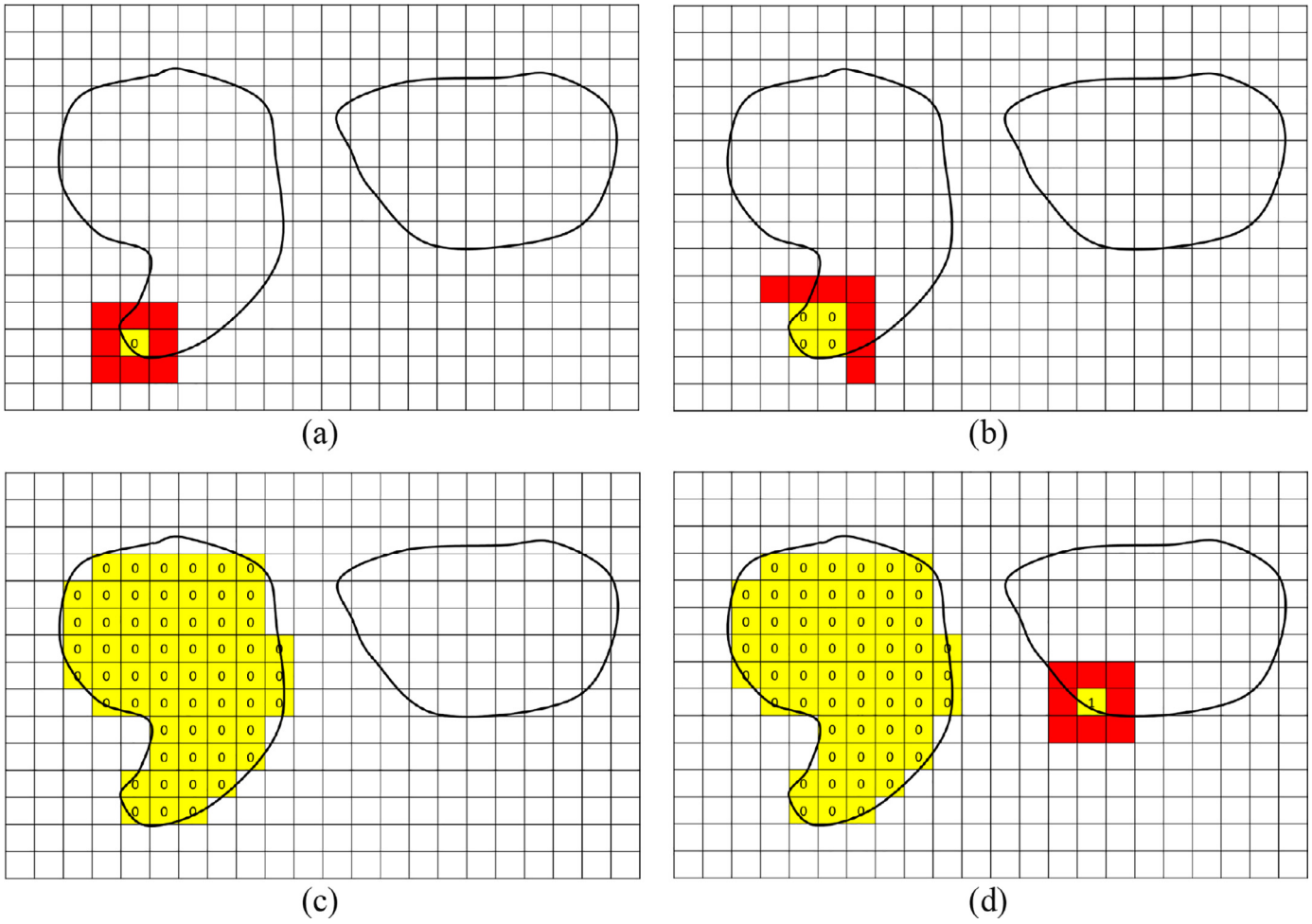

Fig. 3. Illustration of the flood-fill algorithm used for the identification of VOF bubbles. (a) A cell with $\alpha_V < 0.5$ (yellow) is tagged as "0", seeking is performed in its neighbor cells (red). (b) Cells in the same bubble with the initial cell are tagged as "0" and then keep on seeking. (c) The bubble "0" is identified completely. (d) The next bubble "1" begins to be identified. (For interpretation of the references to colour in this figure legend, the reader is referred to the web version of this article.)

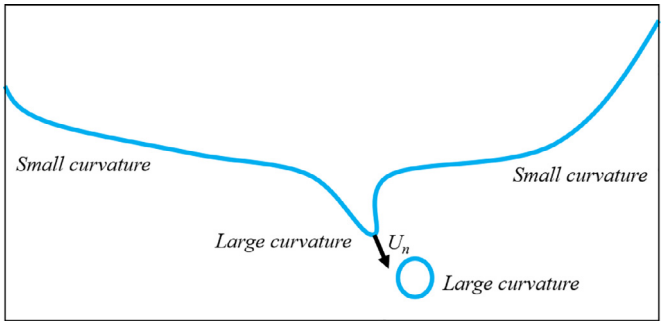

Fig. 4. Illustration of the difference of curvature when interface breaking.

by the isosurface $\phi = 0$. The distance function field is obtained by solving the re-initialization equation (Sussman et al., 1998):

$$\begin{cases} \dfrac{\partial \phi}{\partial \tau} = S(\phi_0)(1 - \nabla \phi) \\ \phi(x, 0) = \phi_0(x) = (2\alpha_v - 1) \cdot \Omega \end{cases} \tag{23}$$

where τ is the artificial time step, $S(\varphi_0)$ is a sign function, Ω is a small value defined as $0.75\Delta x$ where Δx is grid size. The initial value of Level-set function is constructed by the volume fraction in VOF method. The solution converges to a signed distance function achieving $|\phi| = 1$ after several iterations. The interface normal vector and curvature are then calculated by the ϕ field as:

$$\hat{n} = \frac{\nabla \phi}{|\nabla \phi|} \tag{24}$$

$$k(\phi) = \nabla \cdot \hat{n} \tag{25}$$

Because of the characteristic of continuity, the Level-set function can help calculate the interface curvature and surface tension accurately, which provides a favorable conditions for the implementation of the curvature-based transformation algorithm.

4.3. Computational procedure

In summary, by the combination of the numerical models and algorithms introduced above, the main computational procedure can be seen in Table 1 Before the solving loop begins, initial data containing Lagrange bubble positions and VOF interface and the corresponding volumetric field are calculated. During each time step, behaviors of Lagrange bubbles are evaluated first including breakup, collision and coalescence according to Eqs. (9)–(13). Then the forces acting on the Lagrange bubbles are calculated based on the grid data and the motion is solved based on Eqs. (6)–(8). Multi-scale transformations are implemented next. Lagrange bubbles that come into contact with the air-water interface or that are larger than the critical size will be transformed to the VOF interface as Eqs. (14)–(18). After that, small scale bubbles will be transformed from VOF interface to Lagrange tracking by specific algorithms as Eqs. (19)–(22). Finally is a classic PIMPLE loop to solve the VOF

Table 1
Computational procedure of the multi-scale two phase solver for bubbly flows.

	Simulation Procedure
1	Initialize the Lagrange bubble distribution, calculate the corresponding void fraction α_L in grids
2	Initialize the VOF field, calculate the corresponding void fraction α_V in grids
3	**while** time < endTime **do**
4	Evaluate Lagrange bubble breakup
5	Evaluate Lagrange bubble collision and coalescence
6	Calculate hydrodynamic forces and collision force on Lagrange bubbles, update the bubble locations
7	Evaluate transformation from Lagrange bubbles to VOF interface
8	Evaluate transformation from VOF interface to Lagrange bubbles
9	**PIMPLE loop**
10	Solve VOF phase transport equation
11	Solve velocity and pressure equations
12	time += Δt
13	**end while**

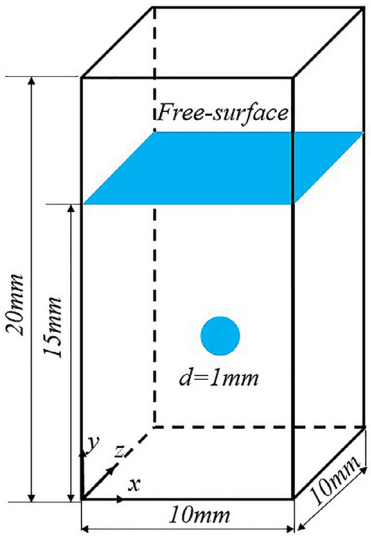

Fig. 5. Numerical conditions for the case that bubble rise up and collide with free-surface.

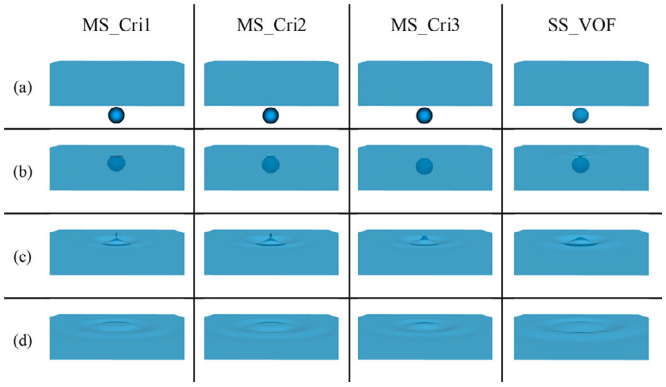

Fig. 6. Multi-scale simulation of bubble rising up and merging with free-surface by three different transformation criteria. (a). Lagrange bubble rise up. (b). Transformation moment from Lagrange bubble to VOF interface. (c). Jet flow at the center of the free-surface after the bubble merges into the interface. (d). Circular ripple on the free surface at the end of simulations.

phase transport equation and N-S equations. The solver is developed based on the open source platform *OpenFOAM*.

5. Results and discussion

This paper focuses on the simulation effect of the multi-scale transformation. In this section, the ability of the present solver will be presented by typical academic cases. At the same time, the comparison of different critical criteria, algorithms will be discussed in detail in the simulations.

5.1. Bubble rise up and merge with free-surface

In this section, the solver is validated by simulating the interaction between a rising bubble and free-surface. The test case is derived from the first scenario of the transformation from Lagrange bubbles to VOF interface as Section 4.1 introduced. The numerical conditions can be seen in Fig. 5. The computational domain is a box with 10 mm in length, 10 mm in width and 20 mm in height. An air-water interface is initialized at height 15 mm. A three-dimensional bubble initially at rest is immersed into the water and is located 10 m away from the free-surface. Diameter of the initial bubble is 1 mm and the physical properties are $\rho_b = 1\text{kg/m}^3$ and $\nu_b = 1.48 \times 10^{-5}\text{m}^2/\text{s}$. For the water phase, the physical properties are $\rho_w = 1000\text{kg/m}^3$ and $\nu_w = 1 \times 10^{-6}\text{m}^2/\text{s}$. The computational domain is discretized using $N_x \times N_y \times N_z = 80 \times 160 \times 80$ grid points in three directions. The grid distribution corresponds to 8 grids in a bubble diameter, which is not a fine grid arrangement for a VOF bubble rising up simulation, but it is basically conforms to the resolution of micro-bubbles in the simulation of practical complex problems. The main purpose of this simulation is to verify the performance of different transformation criteria and show the advantages of the multi-scale method in the case with insufficient grid resolution.

As introduced in the Section 4.1, there are three kinds of critical criteria that have been used in the previous studies. However, there is a lack of research on the effect of these criteria on the multi-scale transformation process. Therefore, in order to perform this work, three multi-scale simulations are carried out as:

- [MS_C*ri*1]: Simulated by multi-scale solver and the critical criterion is $\Delta_{BI} < \Delta_{BI}^{cri} = d/2$ as Eq. (14).
- [MS_C*ri*2]: Simulated by multi-scale solver and the critical criterion is $\Delta_{BI} < \Delta_{BI}^{cri} = d/2 + l_g$ as Eq. (15).
- [MS_C*ri*3]: Simulated by multi-scale solver and the critical criterion is $\Delta_{BI} < \Delta_{BI}^{cri} = d/2 + 2l_g$ as Eq. (16).

In order to investigate the simulation effect of the multi-scale solver in contrast with the traditional single-scale solver, a VOF simulation is carried out under the same conditions with the above multi-scale simulations. The results are called SS_VOF in the following figures.

First, three multi-scale simulation results in Fig. 6 are discussed. During the rising process shown in Fig. 6(a), the bubble is modeled as a spherical Lagrange particle. The hydrodynamic forces acting on the bubble is quickly balanced and the bubble maintains a steady rising velocity. Fig. 6(b) shows the transformation moment

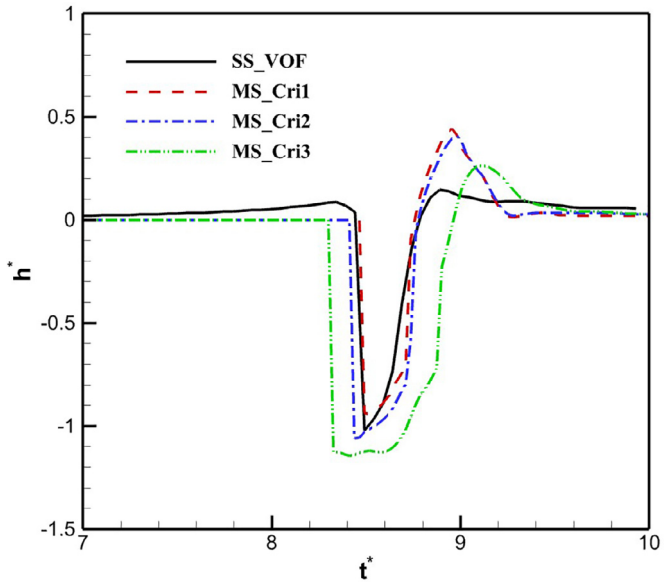

Fig. 7. Comparison of the diachronic evolution of the center height of the free-surface between three multi-scale transformation simulations and one single-scale simulation.

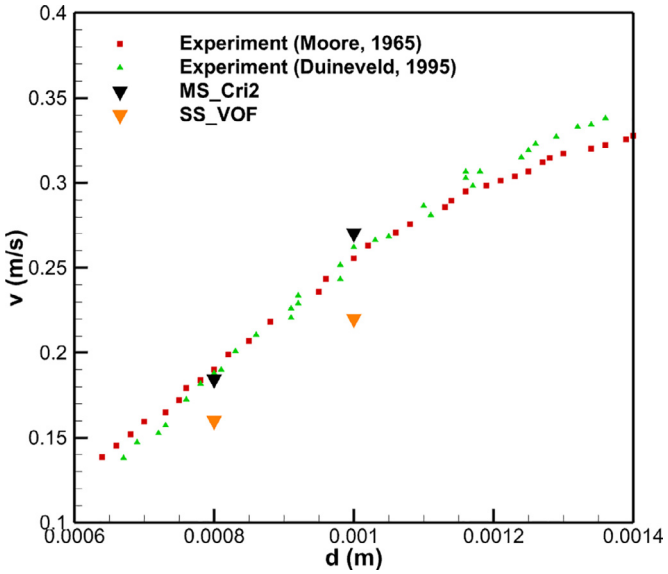

Fig. 8. Comparison of final velocity of bubbles rising up in quiescent water.

in the simulations. The original Lagrange bubble can be successfully transformed into a VOF bubble with interface capturing. Obvious differences can be seen from the results of three different cases. Because of the adoption of different criteria, the transformation is successively advanced in these cases. The transformation in case MS_Cri1 takes place at the latest, at which time the Lagrange bubble has overlapped with the free-surface, leading to a certain amount of mass loss. On the other hand, the transformation in case MS_Cri1 takes place too early. Due to the less grid resolution, the early transformation will first bring some oscillation on the bubble surface, which will affect the bubble movement. In contrast, the transformation moment of case MS_Cri2 is relatively reasonable, at which time the Lagrange bubble is just in contact with the free surface. Fig. 6(c) presents the jet flow at the center of the free-surface after the bubble merges into the interface. Separated droplets can be seen clearly in the case MS_Cri1 and MS_Cri2. However, the phenomenon is not captured in the case MS_Cri3. Finally, the jet flow falls back and forms a circular ripple on the free surface as Fig. 6(d) shows. In order to quantitatively compare the influence of three different critical criteria on the evolution of free-surface after transformation, the diachronic evolution of the center height of the free-surface is plotted as shown in Fig. 7.

Fig. 7 presents the diachronic evolution of the center height of the free-surface. The *x*-coordinate is the dimensionless time which is defined as $t^* = tU_b/d$, while the *y*-coordinate is the dimensionless free-surface height which is defined as $h^* = h/d$. The peak of the curve represents the height of the central jet flow. The height results calculated from case MS_Cri1 and MS_Cri2 are close and significantly higher than that calculated from case MS_Cri3. Combined with Fig. 6(c), it can be seen that the increase of jet flow height is reflected by the generation of separated droplets. In the simulation of flow phenomena after multi-scale transformation, case MS_Cri1 and MS_Cri2 are better than MS_Cri3. At the same time, although the simulation effect of the first two cases is not very different, case MS_Cri2 has a slightly better conservation of mass due to its early transformation. Therefore it can be concluded that the corresponding critical criterion $\Delta_{BI} < \Delta_{BI}^{cri} = d/2+l_g$ is better for using in the transformation scenario that Lagrange bubbles contact with an existing interface.

Then, the comparison between multi-scale simulation results of MS_Cri2 and single-scale simulation results of SS_VOF is discussed. In Fig. 6, it can be seen that most of the evolution processes fit well. However, the droplet splash phenomenon captured in the multi-scale simulation is not reproduced by the single-scale simulation. Quantitatively, the comparison of diachronic evolution of the center height of the free-surface between the MS cases and SS_VOF case is also plotted in Fig. 7. Comparing the results of case SS_VOF with case MS_Cri2, the merge time and the valley value of the curve of the two simulation results are in good agreement. However, significant difference can be seen in the central jet flow height. Result of the case SS_VOF is much smaller than that of the multi-scale case. It has been proposed by previous related studies that the jet flow height depends sensitively on the bubble velocity. Therefore, the final velocities of the rising bubbles in two kinds of simulations are plotted in Fig. 8 for further analysis.

Fig. 8 presents the final velocity of rising bubbles. Since the bubble rising up in quiescent water is a classic problem, two experimental measurement data (Moore, 1965; Duineveld, 1995) are also plotted to validate the numerical results. It can be found that the rising velocity of case MS_Cri2 agrees better with the experimental results, while the rising velocity of case SS_VOF is obviously lower. As introduced above, the grid distribution used in the simulation corresponds to 8 grids in a bubble diameter. Insufficient grid resolution causes a certain degree of errors in the SS_VOF simulation of rising bubble. The under-predicted rising velocity is the main reason why the height of central jet flow is lower in the SS_VOF case as shown in Fig. 7. In contrast, the motion of bubbles tracked under the Lagrange framework is obtained by a series of force models, so it can still predict the velocity accurately with less grid resolution. The accurate predicted rising velocity makes it better to capture the flow phenomenon after the multi-scale transformation as Fig. 6 shows. It can be seen clearly how the multi-scale solver is better than the single-scale pure VOF method as the bubble becomes less resolved.

5.2. Bubble coalesces and exceed a critical scale

In this section, the simulation effect of transformation from Lagrange bubbles exceeding critical scale to VOF interface is verified. The test case is derived from the second scenario of the transformation from Lagrange bubbles to VOF interface as Section 4.1 introduced. The numerical conditions can be seen in Fig. 9. A rectangular vertical channel with a side length of 9 mm is used as the

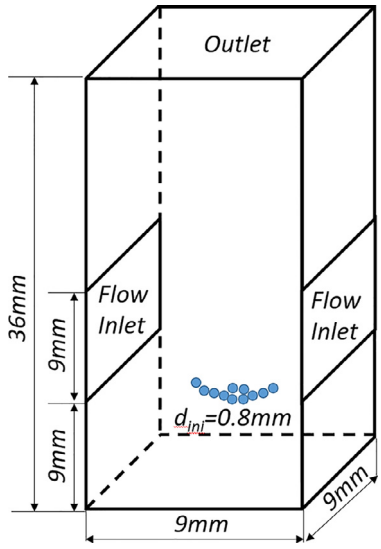

Fig. 9. Numerical conditions for the case of bubble coalescence.

computational domain. The height of the domain is 36 mm, and two water flow inlet boundaries with the velocity of 0.035 m/s are arranged symmetrically on the left and right sides. The computational domain is discretized using $N_x \times N_y \times N_z = 90 \times 360 \times 90$ grid points in three directions. 12 bubbles with the diameter of 0.8 mm are randomly initialized near the height of 4.5 mm. The flows on both sides are used to push the rising bubbles to contact with each other. Density and viscosity of the fluids are set to be the same with those in the Section 5.1. The initial conditions are selected after several tests, aiming at creating a simulation effect that a part of the micro-bubbles coalesce and form large bubbles over a critical scale. The critical bubble diameter is set to be 1.5 mm in the present simulation, which means that the Lagrange bubbles larger than 1.5 mm will be transformed to VOF interface.

Evolution of bubble behaviors in the vertical channel is presented in Fig. 10. Initially, some of the Lagrange bubbles are in contact with each other. By using the coalescence model introduced in Section 3.4, the micro-bubbles soon coalesce and become medium-sized bubbles. Driven by the water flow on both sides, the bubbles move toward the center as the rising process. Two larger Lagrange bubbles contact and then form a bubble with a diameter of more than 1.5 mm. The bubble in the present flow field should be deformed, which is not in line with the spherical bubble hypothesis of the Lagrange bubble tracking method. Therefore, the bubble after coalescence is directly transformed into the VOF interface within one time step as the Fig. 10(c) and 10(d) show. After the multi-scale transformation, the shape of VOF bubbles gradually changes from sphere to ellipsod. The rising velocity of the ellipsoidal bubble is slightly lower than that of the original spherical bubble, which conforms to the actual physical phenomenon.

Table 2
Physical parameters and non-dimensional numbers defining the test case.

ρ_l	ρ_b	μ_l	μ_b	g	σ	Re	Eo	ρ_l/ρ_b	μ_l/μ_b
1000	1	10	0.1	0.98	1.96	35	125	1000	100

5.3. Large bubble rising and breakup

In this section, rising and breakup process of a large bubble are simulated to validate the transformation algorithm from VOF interface capturing to Lagrange tracking of the multi-scale solver. The test case is performed against Hysing et al.'s (2009) quantitative benchmark computations of two-dimensional bubble rising. Two benchmark cases were provided in their paper, and the more challenging one with larger density ratio and complex breakup is adopted for the simulation of this section. The numerical conditions can be seen in Fig. 11. A bubble with the diameter of 0.5 centered at the position (0.5, 0.5) in a 1×2 rectangular computational domain. The computational domain is discretized using $N_x \times N_y = 80 \times 160$ grid points. No-slip boundary condition is adopted for the upper and lower wall, while free-slip boundary condition is used for the vertical walls. Table 2 presents the physical parameters and non-dimensional numbers defining the test case, where the Reynolds number is defined as $Re = \rho_l \sqrt{gd} d/\mu_l$ and the Eötvös number is defined as $Eo = \rho_l g d^2/\sigma$. In the rising process, the original bubbles will break up and then shed out micro-bubbles and

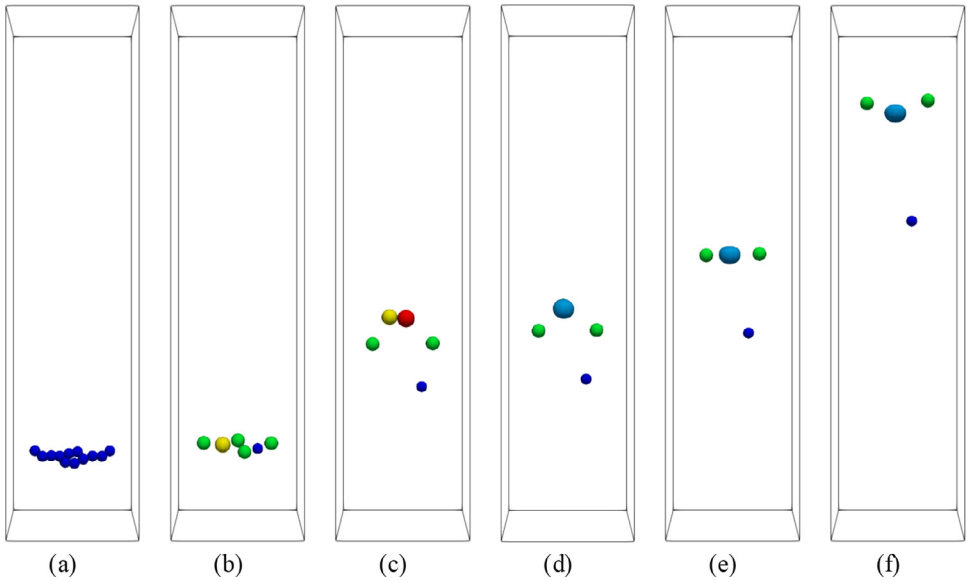

Fig. 10. Multi-scale simulation of the bubble coalescence and exceed a critical scale. (a). Initial distribution of the Lagrange bubbles. (b). Some contacted micro-bubble coalesce to middle-sized bubbles. (c). Two larger bubbles contact driven by the lateral water flow. (d). Lagrange bubble exceeding the critical scale after coalescence is transformed into VOF interface capture. (e). The shape of large VOF bubble becomes ellipsoidal. (f). Final flow state.

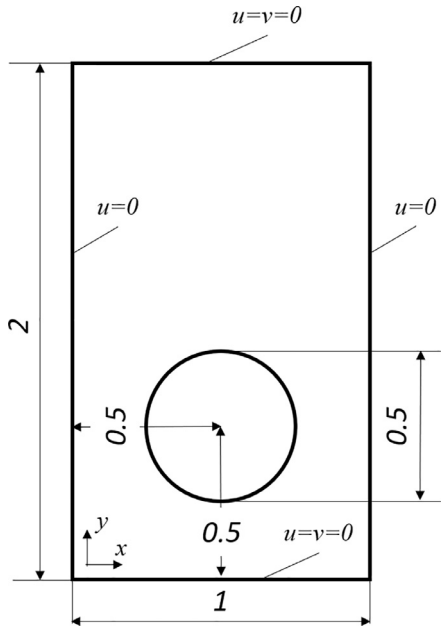

Fig. 11. Numerical conditions of the case that two-dimensional large bubble rising and breakup.

banded flow structure, which present challenges to the traditional interface capture methods.

As introduced in the Section 4.2, most of the previous multi-scale solvers adopted the identify-based algorithm for the transformation form VOF interface to Lagrange bubbles [17, 25]. This algorithm is realized by a flood-fill idea in the present solver. In addition, a new curvature-based transformation algorithm is proposed in this paper. In order to compare the performance of different algorithms, three simulations are carried out as:

- [MS_IBA]: Simulated by multi-scale (MS) solver combined with the identify-based algorithm (IBA).
- [MS_CBA]: Simulated by multi-scale (MS) solver combined with the curvature-based algorithm (CBA).
- [SS_VOF]: Simulated by single-scale solver and the interface is captured by VOF method.

Fig. 12 shows the results of rising bubble behavior up to $t = 4$ s, given by the case SS_VOF. The bubble is presented by the contour line of $\alpha_V = 0.5$. During the rising process, the bottom of the bubble appears to sag gradually. Thin filaments come out and break off from the edge of the bubble. The time of breakup predicted in the simulation is about $t = 3$ s as Fig. 12(c) shows. Finally, there are only the original main bubble and two middle-sized break off daughter bubbles in the computational domain. It should be noted that the VOF result is obtained using a relatively coarse grid distribution. Micro-scale bubbles are not captured due to the numerical diffusion. In fact, there are some small satellite bubbles trailing the bulk of the main bubble, which has been partly captured by some simulations with high grid resolution in the reference [40].

Fig. 13 shows the bubble behaviors of the case MS_IBA from $t = 3$ s to $t = 4$ s. Results before $t = 3$ s are not presented because no transformation takes place at that time. The critical criterion is set to be $N_b < N_{cri} = 10$, which means that VOF bubbles contained less than 10 grids will be transformed to Lagrange tracking. It can be seen from Fig. 13(b) that in addition to the two middle-sized bubbles breaking off first, there are subsequent micro-scale bubbles that further break off from the original main bubble. These micro-scale two phase flow structures are gradually blurred in the SS_VOF simulation because of the numerical diffusion of traditional VOF methods under less grid resolution. However, the micro-bubbles are successfully captured in the case MS_IBA as shown in Fig. 13(c). By using the multi-scale transformation algorithm, the bubbles that are about to diffuse away are transformed to Lagrange particles. Finally, the simulation of MS_IBA case capture two more spherical bubbles than that of the SS_VOF case.

The results of bubble behaviors calculated from the case MS_CBA are shown in Fig. 14. Critical curvature radius in the curvature-based transformation algorithm is set to be d/50. Distinct difference can be seen in the wake of the main bubble. As the simulation progresses, the micro-scale satellite bubbles continuously break off from the edge of the main bubble and are transformed to Lagrange particles by the multi-scale solver. The Lagrange bubbles breaking off vary in size. In addition, coalescence and breakup can be further accomplished by specific algorithms in the solver. The micro-scale satellite bubbles arrange in long thin trailing filament and trail the bulk of the main bubble. The successful capture of these phenomena shows the excellent simulation effect of curvature-based transformation algorithm proposed in this paper for multi-scale two-phase bubbly flow problems.

The diffusion of phase interface is a key problem in the simulation of multi-scale two-phase flow problems using the traditional algebraic VOF method. If a constant isosurface of volume fraction is used to represent the bubbles in the flow field, the size of the bubbles will gradually decrease, and the micro-scale bubbles will gradually disappear. This phenomenon is more obvious

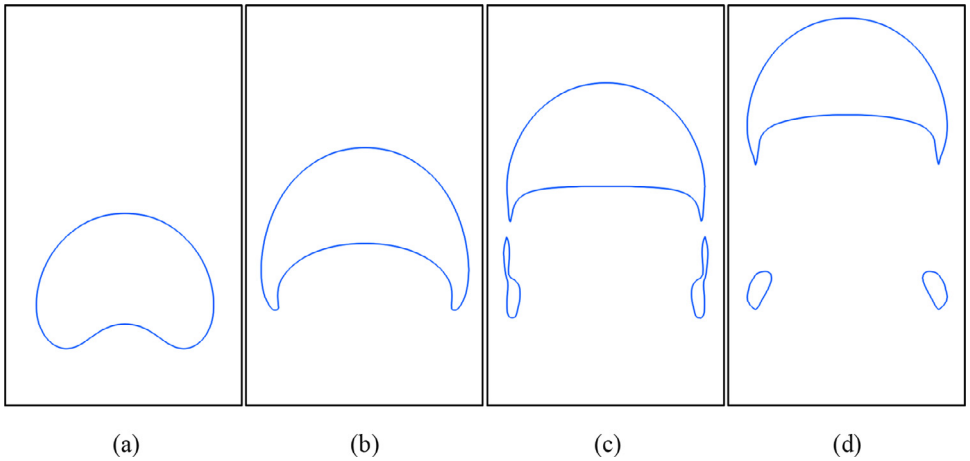

Fig. 12. Simulation results of rising bubble behavior given by the case SS_VOF. (a). $t = 1$ s. (b). $t = 2$ s. (c). $t = 3$ s. (d). $t = 4$ s.

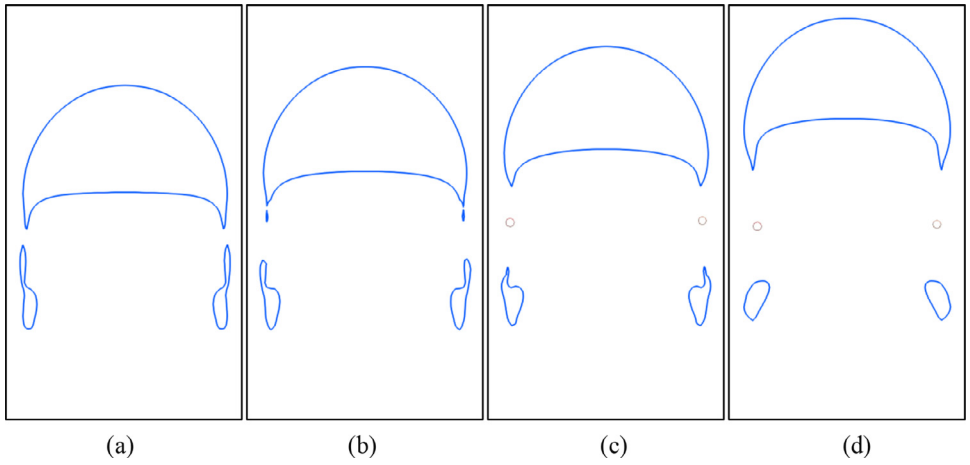

Fig. 13. Simulation results of rising bubble behavior given by the case MS_IBA. (a). $t = 3$ s. (b). $t = 3.25$ s. (c). $t = 3.58$ s. (d). $t = 4$ s.

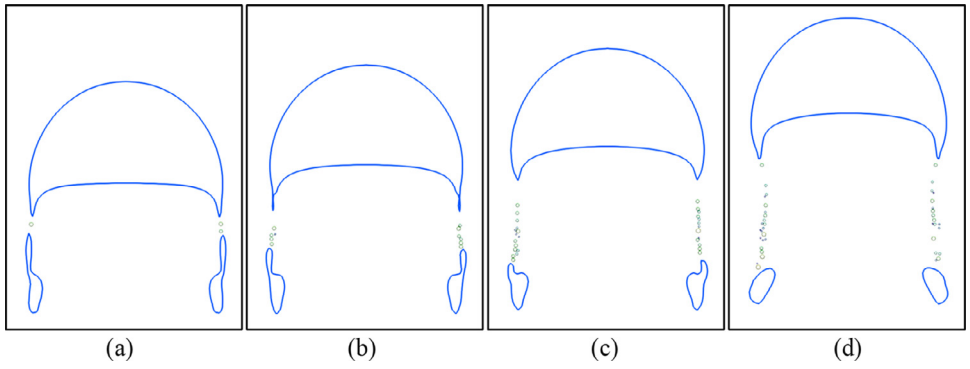

Fig. 14. Simulation results of rising bubble behavior given by the case MS_CBA. (a). $t = 3$ s. (b). $t = 3.25$ s. (c). $t = 3.5$ s. (d). $t = 4$ s.

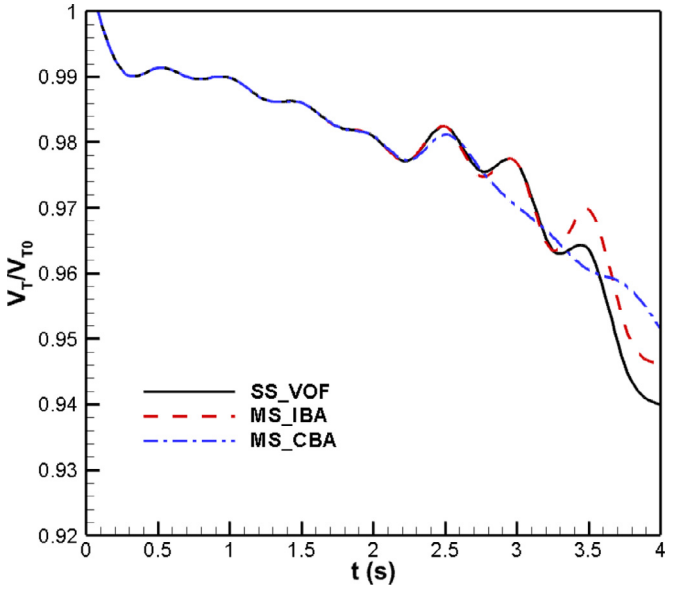

Fig. 15. Total volume of bubbles in the flow field varies over time.

at less grid resolution. Fig. 15 shows the total volume of bubbles in the flow field varying over time in the simulation. V_T is calculated by adding the volume contained in the isosurface $\alpha_V = 0.5$ and the volume of Lagrange bubbles in the flow field. V_{T0} is the initial volume of the main bubble. It can be seen that the multi-scale simulation method using the two transformation algorithms can compensate the bubble volume loss in the flow field to a certain degree. After the break-off of small bubbles, the volume loss is more dramatic in the case SS_VOF because the small bubbles cannot be captured at less grid resolution. However, the volume of the breaking off bubbles are collected by the multi-scale solver using Lagrange tracking. Therefore the volume losses of case MS_IBA and MS_CBA are smaller than that of the case SS_VOF. In contrast, the curvature-based transformation algorithm proposed in this paper performs better for keeping the volume at the final time, because more bubbles are captured in the wake of the main bubble as Fig. 14 shows.

Computational efficiency is an important advantage of curvature-based algorithm in contrast with the identify-based algorithm for the transformation from VOF interface capturing to Lagrange tracking. Fig. 16 summarizes the final simulation effects of the three test cases and the CPU time required to obtain the corresponding results. At the same time, a much finer SS_VOF case with $N_x \times N_y = 320 \times 640$ grid points is performed and the final simulation effect is also plotted. $T_{CPU}^{SS\_VOF\_80\times160}$ is the total CPU time cost in the case SS_VOF with $N_x \times N_y = 80 \times 160$ grid points, and it is used as a benchmark to evaluate the computational efficiency of the multi-scale solver. The cases are performed serially using an Intel Core i7–7700 CPU. It costs 148 s of CPU time to complete the computation of case SS_VOF_80 × 160. It is obvious in Fig. 16 that the computational cost of case MS_IBA is much larger than that of case SS_VOF. The direct reason is that it takes a lot of computational time to identify the VOF bubbles in the flow field at each time step. In the identification process, seeking and evaluating the neighbor grids are bound to carry out a lot of loops, whatever the algorithm is recursive or not. If there are bubbles in the flow field that contain a large number

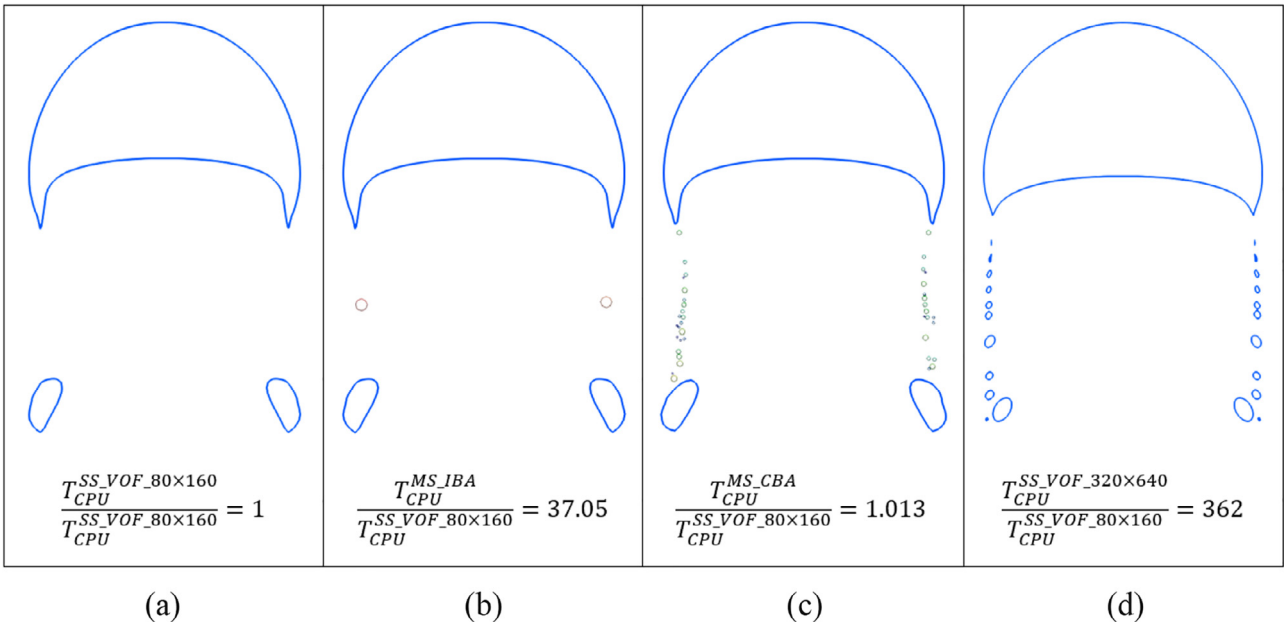

Fig. 16. Summary of the final simulation effects of the four test cases and the CPU time required to obtain the corresponding results. (a). Case SS_VOF with 80 × 160 grid points. (b). Case MS_IBA. (c). Case MS_CBA. (d). Case SS_VOF with 320 × 640 grid points. (For interpretation of the references to colour in this figure, the reader is referred to the web version of this article.)

of grids, the identification process will be significantly slowed down because the number of loops nested is too high. In the recent studies of Zuzio et al. [25], they also pointed out that the identification process is time-consuming. Although the simulation effect is indeed improved slightly by comparing Fig. 16(b) with Fig. 16(a), it is not a good choice to add so much computational cost.

It can be seen from Fig. 16(d) that many small bubbles in the wake of the large bubble can also be captured using SS_VOF with further grid refinement. As the grid resolution increases, the time step decreases accordingly, resulting in a more than hundred-fold increase in computing time. The advantage of the curvature-based transformation algorithm can be seen in Fig. 16(c). The capture accuracy of micro-scale bubbles is significantly improved compared with pure VOF simulation with less grid resolution. The phenomenon of small bubbles can be well simulated while the CPU time only increases by 1%. The increased computational cost is used for the evaluation of motion, collision and coalescence of Lagrange bubbles. The implement of curvature-based transformation algorithm does not involve redundant loop calculations, thus there is little additional computing time. Both computational accuracy and efficiency taken into consideration, the algorithm is more promising to be extended to solve three-dimensional complex multi-scale two-phase flow problems.

6. Conclusions

In this paper, an improved multi-scale two-phase solver is developed to simulate bubbly flow problems, in which the macro-scale bubbles are captured by VOF method and micro-scale bubbles are modeled by Lagrange tracking. The dynamic behavior of multi-scale bubbles in incompressible flows is considered comprehensively in the solver, including motion, collision, coalescence and breakup. This paper focuses on the comparison between the simulation effect of multi-scale method and that of pure VOF method, as well as the discussion of multi-scale transformation process and algorithms. Following conclusions can be obtained:

(1) The new multi-scale two-phase model combines the advantage of interface capture method and particle tracking method successfully. The bubbles of different scales in the flow field can be calculated simultaneously by different methods. And the transformation between micro-scale Lagrange tracking and macro-scale VOF capturing is smooth and physical reasonable. The multi-scale two-phase model performs significantly better than the pure VOF model in capturing micro-scale phenomenon under less grid resolution. Especially for the sub-grid bubbles, they directly disappear in the pure VOF simulation due to numerical diffusion, but can be captured by Lagrange tracking in the multi-scale two-phase model. Refining grids to capture micro-scale flow structures is strictly limited by computational costs. But Lagrange method can track arbitrarily small bubbles. Therefore, the multi-scale two-phase model is more promising for the simulation of actual complex two-phase flows.

(2) Comparison is carried out between three different critical criteria for the transformation from Lagrange bubble tracking to VOF interface capturing The criterion $\Delta_{BI} < \Delta_{BI}^{cri} = d/2+l_g$ based on the distance between Lagrange bubbles and existing VOF interface is recommended according to the presented numerical results. The transformation process can be completed smoothly. The dynamic evaluation of the air-water interface can be well simulated with relatively good mass conservation.

(3) A new curvature-based algorithm is proposed for the transformation from VOF interface capturing to Lagrange bubble tracking. The simulation effect and computational time are compared with the previous identify-based algorithm in detail. In conclusion, the advantage of the identify-based algorithm is that the transformation idea is straightforward, VOF bubbles containing many grids can be directly transformed into a Lagrange bubble. However, the disadvantage of the identify-based algorithm is that bubble identification needs to be performed at each time step. A lot of loops are required to seek and evaluate the neighbor grids, which is very time-consuming. For the curvature-based algorithm proposed in this paper, it shows significantly better performance both in simulation precision and computational efficiency. In the given test cases, micro-bubble distribution and flow details are well captured with

computational time increasing by only 1%. The results indicate that the new curvature-based algorithm is more promising to be adopted in actual complex two-phase flow simulation. On the other hand, the main shortcoming of the proposed algorithm is that it is relatively difficult to determine an appropriate control parameter before calculation. Over-breakup may occurs for the VOF interface. Future works will further deal with this problem.

Declaration of Competing Interest

Our research interest is mainly on computational marine hydrodynamics, numerical marine basin, two phase flows, bubble flows, foam flows, fluid-structure interaction, nonlinear wave theory, wave loads on structures, as well as high performance computation on complex ship and ocean engineering flows, etc.

Acknowledgments

This work is supported by the National Natural Science Foundation of China (51909160, 51879159, 51809169), The National Key Research and Development Program of China (2019YFB1704200, 2019YFC0312400), Chang Jiang Scholars Program (T2014099), Innovative Special Project of Numerical Tank of Ministry of Industry and Information Technology of China (2016-23/09), to which the authors are most grateful.

References

Albadawi, A., Donoghue, D.B., Robinson, A.J., et al., 2013. . Influence of surface tension implementation in volume of fluid and coupled volume of fluid with level set methods for bubble growth and detachment. Int. J. Multiphase Flow 53, 11–28.
Alkharabsheh, S., Fernandes, J., Gebrehiwot, B., et al., 2015. . A brief overview of recent developments in thermal management in data centers. J. Electron. Packag. 137, 040801.
Armandoost, P., Morteza, B., Nadooshan, A.A., 2018. Study of the motion of a spheroidal drop in a linear shear flow. J. Mech. Sci. Technol. 32, 2059–2067.
Bihs, H., Kamath, A., Chella, M.A., et al., 2016. A new level set numerical wave tank with improved density interpolation for complex wave hydrodynamics. Comput Fluids 140, 191–208.
Chen, X., Wang, J., Li, J., 2016. Multiscale modeling of rapid granular flow with a hybrid discrete-continuum method. Powder Technol. 304, 177–185.
Chen, X., Wang, J., 2017. Dynamic multiscale method for gas-solid flow via spatiotemporal coupling of two-fluid model and discrete particle model. AIChE J. 63, 3681–3691.
Chen, X., Wang, J., 2018. Mesoscale-structure-based dynamic multiscale method for gas-solid flow. Chem. Eng. Sci. 192, 864–881.
Deike, L., Melville, W., Popinet, S., 2016. Air entrainment and bubble statistics in breaking waves. J. Fluid Mech. 801, 91–129.
Duineveld, P.C., 1995. The rise velocity and shape of bubbles in pure water at high Reynolds number. J. Fluid Mech. 292, 325–332.
Dumouchel, C., Blaisot, J.B., Bouche, E., et al., 2015. Multi-scale analysis of atomizing liquid ligaments. Int. J. Multiphase Flow 73, 251–263.
Grew, K.N., Chiu, W.K.S., 2012. A review of modeling and simulation techniques across the length scales for the solid oxide fuel cell. J. Power Sources 199, 1–13.
Hänsch, S., Lucas, D., Krepper, E., et al., 2012. A multi-field two-fluid concept for transitions between different scales of interfacial structures. Int. J. Multiphase Flow 47, 171–182.
Heitkam, S., Sommer, A.E., Drenckhan, W., et al., 2017. . A simple collision model for small bubbles. J. Phys.: Condensed Matter 29, 124005.
Herrmann, M., 2010. A parallel Eulerian interface tracking/Lagrangian point particle multi-scale coupling procedure. J. Comput. Phys. 229, 745–759.
Hirt, C.W., Nichols, B.D., 1981. Volume of fluid (VOF) method for the dynamics of free boundaries. J. Comput. Phys. 39, 201–225.
Höhne, T., Deendarlianto, A., Lucas, D., 2011. Numerical simulations of counter-current two-phase flow experiments in a PWR hot leg model using an area density model. Int. J. Heat Fluid Flow 32, 1047–1056.
Hsiao, C.T., Ma, J., Chahine, G.L., 2017. Multiscale tow-phase flow modeling of sheet and cloud cavitation. Int. J. Multiphase Flow 90, 102–117.
Hsiao, C.T., Wu, X., Ma, J., 2013. Numerical and experimental study of bubble entrainment due to a horizontal plunging jet. Int. Shipbuild. Progress 60, 435–469.
Hysing, S., Turek, S., Kuzmin, D., 2009. Quantitative benchmark computations of two-dimensional bubble dynamics. Int. J. Numer. Methods Fluids 60, 1259–1288.
Jain, D., Kuipers, J.A.M., Deen, N.G., 2014. Numerical study of coalescence and breakup in a bubble column using a hybrid volume of fluid and discrete bubble model approach. Chem. Eng. Sci. 119, 134–146.
Karimi, K., Marchisio, D., Laurini, E., et al., 2018. Bridging the gap across scales: coupling CFD and MD/GCMC in polyurethane foam simulation. Chem. Eng. Sci. 178, 39–47.
Kuiper, G., 2010. Cavitation in Ship Propulsion. Delft University of Technology.
Lau, Y., Ba, W., Deen, N., et al., 2014. Numerical study of bubble break-up in bubbly flows using a deterministic Euler–Lagrange framework. Chem. Eng. Sci. 108, 9–22.
Li, L., Li, B., Liu, Z., 2017. Modeling of gas-steel-slag three-phase flow in ladle metallurgy: part II. multi-scale mathematical model. ISIJ Int. 57, 1980–1989.
Ling, Y., Zaleski, S., Scardovelli, R., 2015. Multiscale simulation of atomization with small droplets represented by a Lagrangian point-particle model. Int. J. Multiphase Flow 76, 122–143.
Liu, H., Zhang, C., Gao, P., et al., 2018. On the maximal spreading of impacting compound drops. J. Fluid Mech. 854, R6.
Liu, M., Hu, Z., Li, J., 2004. Multi-scale characteristics of chaos behavior in gas-liquid bubble columns. Chem. Eng. Commun. 191, 1003–1016.
Lubin, P., Glockner, S., 2015. Numerical simulations of three-dimensional plunging breaking waves: generation and evolution of aerated vortex filaments. J. Fluid Mech. 767, 364–393.
Ma, J., Chahine, G.L., Hsiao, C.T., 2015b. Spherical bubble dynamics in a bubbly medium using an Euler–Lagrange model. Chem. Eng. Sci. 128, 64–81.
Ma, J., Hsiao, C.T., Chahine, G.L., 2017. A physics based multiscale modeling of cavitating flows. Comput. Fluids 145, 68–84.
Ma, J., Oberai, A.A., Drew, D.A., et al., 2011a. A comprehensive sub-grid air entrainment model for RaNS modeling of free-surface bubbly flows. J. Comput. Multiphase Flows 3, 41–56.
Ma, J., Oberai, A.A., Lahey, R.T., et al., 2011b. Modeling air entrainment and transport in a hydraulic jump using two-fluid RANS and DES turbulence models. Heat Mass Transf. 47, 911–919.
Ma, T., Ziegenhein, T., Lucas, D., 2015a. Euler-Euler large eddy simulations for dispersed turbulent bubbly flows. Int. J. Heat Fluid Flow 56, 51–59.
Mohamed, K.M., Mohamad, A.A., 2010. A review of the development of hybrid atomistic-continuum methods for dense fluids. Microfluid Nanofluid 8, 283–302.
Moore, D.W., 1965. The velocity of rise of distorted gas bubbles in a liquid of small viscosity. J. Fluid Mech. 23, 749–766.
Nambiar, D.K.R., Kumar, R., Das, T.R., et al., 1992. A new model for the breakage frequency of drops in turbulent stirred dispersions. Chem. Eng. Sci. 47, 2989–3002.
Patkar, S., Aanjaneya, M., Karpman, D., et al., 2013. A hybrid Lagrangian-Eulerian formulation for bubble generation and dynamics. In: Proceedings of the 12th ACM SIGGRAPH/Eurographics Symposium on Computer Animation. Anaheim, California July.
Prince, M.J., Blanch, H.W., 1990. Bubble coalescence and break-up in air-sparged bubble columns. AIChE J. 36, 1485–1499.
Rezende, R.V.P., Almeida, R.A., Ulson, A.A., 2015. A two-fluid model with a tensor closure model approach for free surface flow simulations. Chem. Eng. Sci. 122, 596–613.
Schmidtke, M., Lucas, D., 2008. CFD approaches for modelling bubble entrainment by an impinging jet. Sci. Technol. Nucl. Installations 2009, 148436.
Sussman, M., Fatemi, E., Smereka, P., et al., 1998. An improved level set method for incompressible two-phase flows. Comput. Fluids 27, 663–680.
Tomar, G., Fuster, D., Zaleski, S., et al., 2010. Multiscale simulations of primary atomization. Comput. Fluids 39, 1864–1874.
Tomiyama, A., Celata, G.P., Hosokawa, S., et al., 2002a. Terminal velocity of single bubbles in surface tension force dominant regime. Int. J. Multiphase Flow 28, 1497–1519.
Tomiyama, A., Tamai, H., Zun, I., et al., 2002b. Transverse migration of single bubbles in simple shear flows. Chem. Eng. Sci. 57, 1849–1858.
Tong, Z., He, Y., Tao, W., 2019. A review of current progress in multiscale simulations for fluid flow and heat transfer problems: the frameworks, coupling techniques and future perspectives. 137, 1263–1289.
Wang, Z., Yang, J., Stern, F., 2016. High-fidelity simulations of bubble, droplet and spray formation in breaking waves. J. Fluid Mech. 792, 307–327.
Wardle, K.E., Weller, H.G., 2013. Hybrid multiphase CFD solver for coupled dispersed/segregated flows in liquid-liquid extraction. Int. J. Chem. Eng. 2013, 128936.
Xiang, M., Cheung, S.C.P., Tu, J.Y., et al., 2014. A multi-fluid modelling approach for the air entrainment and internal bubbly flow region in hydraulic jumps. Ocean Eng. 91, 51–63.
Yan, K., Che, D., 2010. A coupled model for simulation of the gas-liquid two-phase flow with complex flow patterns. Int. J. Multiphase Flow 36, 333–348.
Yang, N., Wu, Z., Chen, J., et al., 2011. Multi-scale analysis of gas-liquid interaction and CFD simulation of gas–liquid flow in bubble columns. Chem. Eng. Sci. 66, 3212–3222.
Zhang, X., Wang, J., Wan, D., 2020. Euler–Lagrange study of bubble drag reduction in turbulent channel flow and boundary layer flow. Phys. Fluids 32, 027101.
Zuzio, D., Estivalèzes, J.L., DiPierro, B., 2018. An improved multiscale Eulerian–Lagrangian method for simulation of atomization process. Comput. Fluids 176, 285–301.